Journal of Catalysis 365 (2018) 238–248

Contents lists available at ScienceDirect

Journal of Catalysis

journal homepage: www.elsevier.com/locate/jcat

Catalytic performance of phase-pure M1 $MoVNbTeO_x/CeO_2$ composite for oxidative dehydrogenation of ethane

Dan Dang [1], Xin Chen [1], Binhang Yan, Yakun Li, Yi Cheng *

Department of Chemical Engineering, Tsinghua University, Beijing 100084, PR China

ARTICLE INFO

Article history:
Received 7 March 2018
Revised 5 July 2018
Accepted 6 July 2018

Keywords:
Oxidative dehydrogenation of ethane (ODHE)
Ethylene
$MoVNbTeO_x$
Mixed metal oxide
Ceria

ABSTRACT

The introduction of cerium oxide to phase-pure M1 $MoVNbTeO_x$ with CeO_2 loading from 0 up to 90 wt.% results in highly active catalysts for oxidative dehydrogenation of ethane (ODHE). These catalysts are characterized with BET, ICP, XRD, TEM, SEM and XPS techniques and tested for ODHE process. The results show that the increase of active site, V^{5+}, is one of the dominant factors to improve the ethane conversion. In addition, the easier re-oxidation of V^{4+} to V^{5+} due to the presence of Ce^{4+} makes an extra contribution to the increase of turn-over frequency. Among all the catalysts, M1 catalyst with 30 wt.% CeO_2 loading obtains the best productivity of 0.69 $kg_{C2H4}/kg_{cat}\cdot h$ while the corresponding performance of phase-pure M1 catalyst is 0.34 $kg_{C2H4}/kg_{cat}\cdot h$ at 400 °C with the contact time of 18.52 $g_{cat}\cdot h/mol_{C2H6}$. It is further demonstrated that $M1/CeO_2$ catalyst (e.g., with 50 wt.% CeO_2 as a representative) loading remains highly active after 3 cycles of refreshment in situ, and its crystal structure and surface morphology keep stable compared to the fresh catalyst.

1. Introduction

Ethylene is one of the most important building blocks in the chemical industry [1]. The oxidative dehydrogenation of ethane (ODHE) to ethylene has received considerable attention because of its distinct advantages (e.g., thermodynamically favored, lower reaction temperature, no coke formation, etc.) over steam cracking process [2–4]. In recent years, mixed metal oxides seem to be the most promising catalytic system for ODHE reaction [4–14]. Among them, $MoVNbTeO_x$ catalyst exhibits attractive performances (i.e., activity, selectivity and productivity) at the reaction temperature of about 400 °C.

Usually, $MoVNbTeO_x$ catalyst is prepared by slurry method [14–18] or hydrothermal method [4,19,20]. This multicomponent metal oxide is nanocrystalline solid mainly composed of phase-M1 and phase-M2 [21]. The M1 phase has a needle-like crystal morphology in which the (0 0 1) planes are arranged perpendicular to the long axis of the needles [22]. While the M2 phase has characteristic hexagonal rings hosting the Te-O units without any pentagonal or heptagonal rings in the (0 0 1) planes [20,23]. Previous studies have indicated that the M1 phase is the most efficient phase in ethane oxidation, assuming V^{5+} ions as ethane activation sites [4,24,25]. The performance of $MoVNbTeO_x$ catalysts increases with the purity of M1 phase [26]. It is reported that the $MoVNbTeO_x$ catalyst has a considerable potential for industrial application when the catalytic activity obtains ethane conversion >80% and ethylene selectivity >90% [27–30]. However, according to the reported catalysts, the industrial requirements for commercialization (e.g, 1.00 $kg_{C2H4}/kg_{cat}\cdot h$ catalyst productivity) is far from achieved [29]. Since the catalytic activity of phase-pure M1 is related with the amount of V^{5+} ions, increasing their amount could be an important working direction. Meanwhile, because of the expensive raw material for catalyst preparation and mass loss caused by post-treatment, the high cost of $MoVNbTeO_x$ catalysts is one of the crucial reasons hindering the industrial implementation in the ODHE process [11]. As a result, introduction of cheap promoters naturally becomes a simple and effective method for catalyst improvement and cost reduction. At present, α-Al_2O_3, SiO_2, and ZrO_2 have been added into the $MoVNbTeO_x$ catalysts [11,31] as diluters with little influence on the surface chemistry of the composite catalyst [14,31]. In our previous work, the introduction of CeO_2 significantly improved the catalytic efficiency and reduced the cost of catalyst in ODHE process, which provides a promising idea and preliminary verification on improvement of $MoVNbTeO_x$ catalysts. However, further detailed and thorough research on the addition of CeO_2 to $MoVNbTeO_x$ catalysts is still needed.

In this work, M1 $MoVNbTeO_x/CeO_2$ ($M1/CeO_2$) catalysts are synthesized for the ODHE reaction. As a matter of fact, pure CeO_2

* Corresponding author.
E-mail address: yicheng@tsinghua.edu.cn (Y. Cheng).
[1] Dan Dang and Xin Chen contributed equally.

https://doi.org/10.1016/j.jcat.2018.07.016
0021-9517/

shows low activity of ethane conversion and low selectivity to ethylene in the ODHE process at a temperature lower than 500 °C [11,34,35]. However, CeO_2 itself has high oxygen-storage capacity (OSC) and easy oxidation/reduction of the Ce^{4+}/Ce^{3+} redox couple [32,33]. Therefore, the essential idea of this paper is to use CeO_2 as an oxidant, added to the phase-pure M1 catalyst, to increase the number of vanadium active sites so as to improve the catalytic performance [23]. The catalytic performance is evaluated for the ODHE in a laboratory-scale fixed-bed reactor and the characterization of the catalysts are achieved by using XRD, BET, ICP, XPS, SEM and TEM techniques.

2. Experimental section

2.1. Catalyst preparation

$MoVNbTeO_x$ catalysts are prepared by hydrothermal synthesis [11,20,36,37]. Ammonium heptamolybdate (Sigma-Aldrich, 99.0%), vanadyl sulfate (Sigma-Aldrich, 97%) telluric acid (Sigma-Aldrich, 98%) and ammonium niobium oxalate (Sigma-Aldrich, 99.99%) are used to prepare an aqueous slurry comprising Mo, V, Te and Nb at the molar ratio of Mo:V:Te:Nb = 1:0.25:0.23:0.18. The slurry is put into a 100 ml Teflon autoclave, where the air inside the autoclave is replaced by nitrogen for 15 min. Then the autoclave is placed in an oven at 175 °C for 48 h. The obtained suspension is filtered and washed by 500 ml deionized water, dried overnight at 80 °C and calcinated in nitrogen at 600 °C for 2 h with the heating rate of 5 °C/min. The formed lump solid is grinded to powder form, which is the mixture of phases M1 and M2. After removal of phase M2 by using 30% HNO_3, the phase-pure M1 is obtained accordingly.

The $M1/CeO_2$ catalysts are synthesized by a sol–gel method [11]. Cerium nitrate (Sigma-Aldrich, 99%) and citric acid (Sigma-Aldrich, 99.5%) are dissolved in deionized water at a molar ratio of 1:3 with continuous agitation for 24 h at 65 °C and obtained a stable transparent sol with 10 wt.% CeO_2. Powder phase-pure M1 is introduced to the CeO_2 sol at different mass ratios, stirred in 60 °C water bath for 2 h, and dried overnight at 80 °C. Finally, a series of catalysts with 10 wt.%, 20 wt.%, 30 wt.%, 40 wt.%, 50 wt.%, 70 wt.%, 90 wt.% CeO_2 are obtained after the activation by calcination in air for 6 h at 400 °C with the heating rate of 5 °C/min in muffle furnace. The prepared catalysts are named $M1/10CeO_2$, $M1/20CeO_2$, $M1/30CeO_2$, $M1/40CeO_2$, $M1/50CeO_2$, $M1/70CeO_2$, $M1/90CeO_2$, respectively. The pure CeO_2 is also prepared by drying of CeO_2 sol and calcination in air at 400 °C for 6 h. Its catalytic activity is also tested in the ODHE reaction in comparison with other catalysts.

2.2. Catalyst characterization

Metal contents are measured by inductively coupled plasma-optical emission spectrometry (ICP-OES, Varian Vista RL spectrometer).

Specific surface areas of the samples are determined by nitrogen adsorption carried out at 77 K on a Quantachrome Autosorb-6B analyzer. The data are calculated by multipoint BET analysis method in the pressure range of P/P_0 = 0.05–0.30. Prior to the measurement, the samples are degassed in vacuum at 300 °C for 2 h.

X-ray diffraction (XRD) patterns of samples are obtained using a Bruker D8 Advance equipment with Cu Kα radiation. 2θ scans are run from 5 to 70° at a rate of 0.5 degree per minute. The spectra are identified with JCPDS database (Joint Committee of Powder Diffraction Standards) and the ICSD database (Inorganic Crystal Structure Database). M1 phase (ICSD 55097) has characteristic diffraction lines located at 2θ = 6.6°, 7.7°, 8.9°, 22.1°.

The morphology of the synthesized catalysts are studied by scanning electron microscopy (SEM, Zeiss, GeminiSEM 500) and JEOL JEM2010 high-resolution transmission electron microscopy (HR-TEM).

X-ray photoelectron spectra (XPS) measurements with a PHI Quantera SXM system equipped with Al Kα X-ray source are made to analyze the ion concentration on catalyst surface. Survey scans (0–1200 eV) and high-resolution Mo (3d), V (2p), Te (3d), Nb (3d), Ce (3d) and C (1s) spectra are obtained. During the scanning for vanadium and cerium, the dwell time is increased from 300 ms to 500 ms and the number of scan times is increased from 6 to 10. The binding energy scale is corrected by setting the C (1s) signal at 284.8 eV. The XPS data analysis for vanadium is performed with XPSPEAK 4.1 software and that for cerium is performed with Thermal Advantage 4.88 software. The binding energy data of reference materials are obtained from NIST X-ray Photoelectron Spectroscopy Database.

2.3. Catalyst test

All of the catalysts for ODHE reaction are evaluated in a fixed-bed quartz tubular reactor (8 mm i.d., 750 mm in length) heated by a furnace, in which the temperature in the middle of the catalyst bed is measured with a thermocouple. The catalyst particles with 0.3 g in mass are diluted with 3.0 g quartz particles with the size of about 200 μm to achieve the isothermal operation. The feed composition is $30C_2H_6/20O_2/50He$. The contact time is defined as W/F_{C2H6} (W is the catalyst mass and F_{C2H6} is the ethane molar flow rate), and the total flow rate is varied from 22 ml/min to 66 ml/min.

The reactants and products are analyzed with an online Shimadzu GC 2014 gas chromatograph equipped with A PorapakQ column for identifying CO_2, C_2H_4 and C_2H_6 and a 5A molecular sieve column for O_2, N_2, CH_4 and CO. A blank run is conducted by loading the reactor with only quartz sands at the same reaction conditions. No ethane conversion is detected, indicating that the homogeneous gas phase reaction can be neglected.

The conversion of ethane and the selectivity to products are calculated as follows:

$$X_{C_2H_6} = \left(1 - \frac{2f_{C_2H_6}}{2f_{C_2H_6} + 2f_{C_2H_4} + f_{CO} + f_{CO_2}}\right) \times 100\% \quad (1)$$

$$S_{C_2H_4} = \frac{2f_{C_2H_4}}{2f_{C_2H_4} + f_{CO} + f_{CO_2}} \times 100\% \quad (2)$$

$$S_{CO} = \frac{f_{CO}}{2f_{C_2H_4} + f_{CO} + f_{CO_2}} \times 100\% \quad (3)$$

$$S_{CO_2} = \frac{f_{CO_2}}{2f_{C_2H_4} + f_{CO} + f_{CO_2}} \times 100\% \quad (4)$$

where X_{C2H6} is the ethane conversion, S is the selectivity to a certain product, and f is the molar fraction in the effluent gas.

3. Results and discussion

3.1. Catalyst performance for ODHE

3.1.1. Effect of contact time

The performances of catalysts M1 with and without addition of CeO_2 in ODHE process at 400 °C with different contact times are presented in Figs. 1–3. The detailed experiment data tested at 400 °C and 18.52 g_{cat}·h/mol_{C2H6} are listed in Table 1. Each data is collected after 2 h since the change of flow rate. Ethylene, carbon

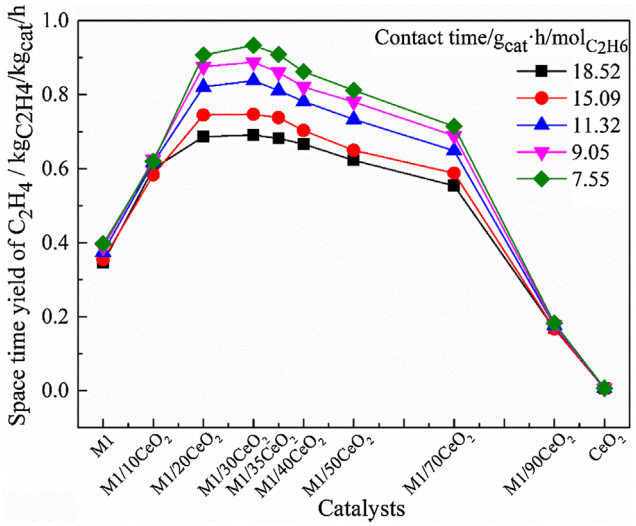

Fig. 1. Space time yield of ethylene as a function of CeO_2 content in ODHE process with different contact times.

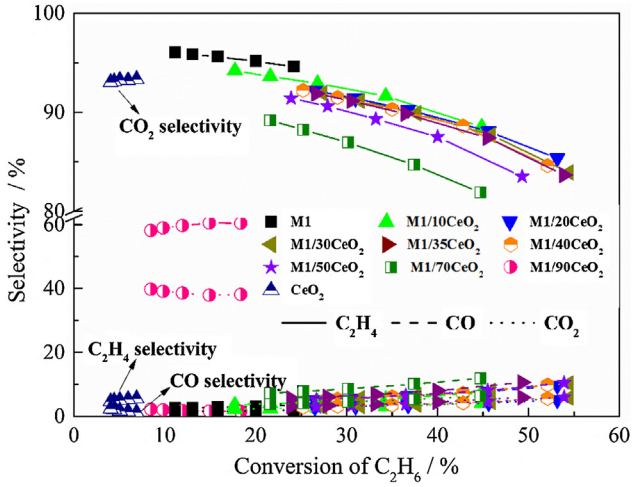

Fig. 2. Ethylene selectivity as a function of ethane conversion in ODHE process with different contact times.

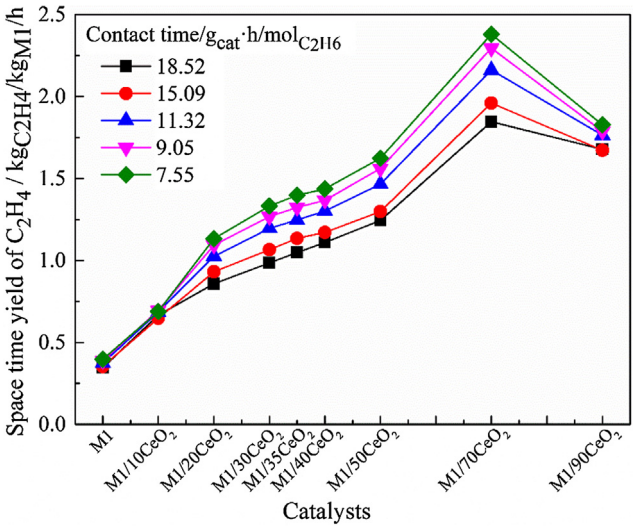

Fig. 3. Space time yield of ethylene as a function of CeO_2 content normalized by M1 content with different contact times.

Table 1
Catalytic performance of catalysts in ODHE process.[a]

Catalysts	C_2H_6 conversion / %	Products distribution/%		
		C_2H_4	CO	CO_2
M1	24.2	94.6	3.5	1.9
M1/30CeO_2	54.4	83.9	10.3	5.8
M1/50CeO_2	49.3	83.5	10.6	5.9
M1/70CeO_2	44.8	81.9	11.8	6.3
M1/90CeO_2	18.4	60.4	1.5	38.1
CeO_2	6.9	5.5	1.1	93.3

[a] Reaction condition: reaction temperature of 400 °C, contact time of 18.52 g_{cat}·h/mol_{C2H6}, C_2H_6/O_2/He molar ratio of 30/20/50 at the reactor inlet.

monoxide and carbon dioxide are the major products in the ODHE process. Meanwhile, little acetic acid exists in the product gases, which is small enough to be ignored, just as reported in the literature [38].

The catalytic performances of these catalysts strongly depend on the incorporation of CeO_2 at the same reaction conditions. Fig. 1 displays a volcano shaped behavior with the CeO_2 addition,

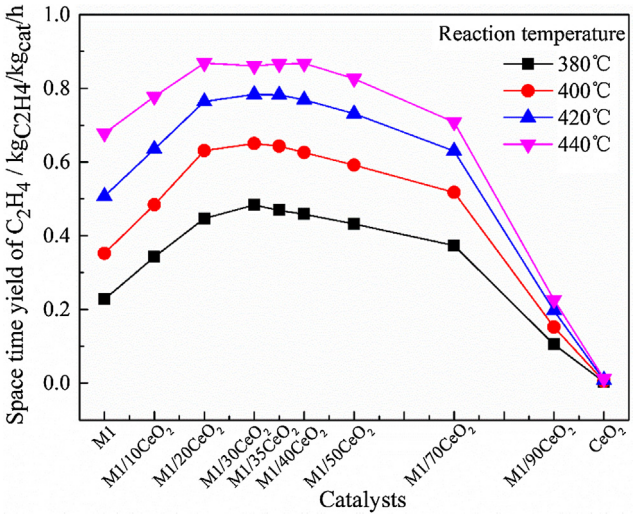

Fig. 4. Space time yield of ethylene as a function of CeO_2 content on M1 in ODHE process.

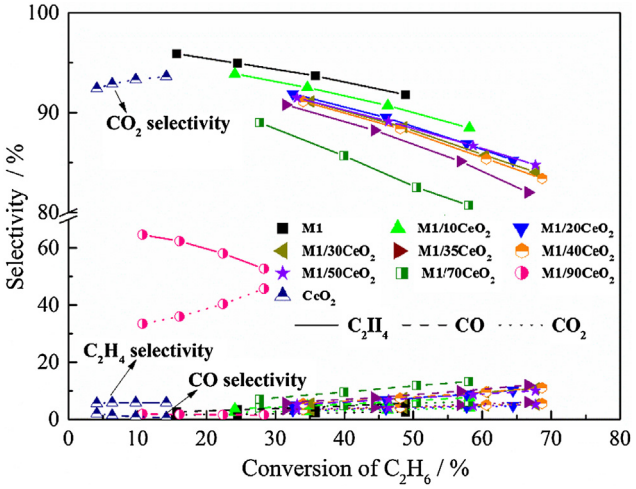

Fig. 5. Ethylene selectivity as a function of ethane conversion in ODHE process at different temperatures.

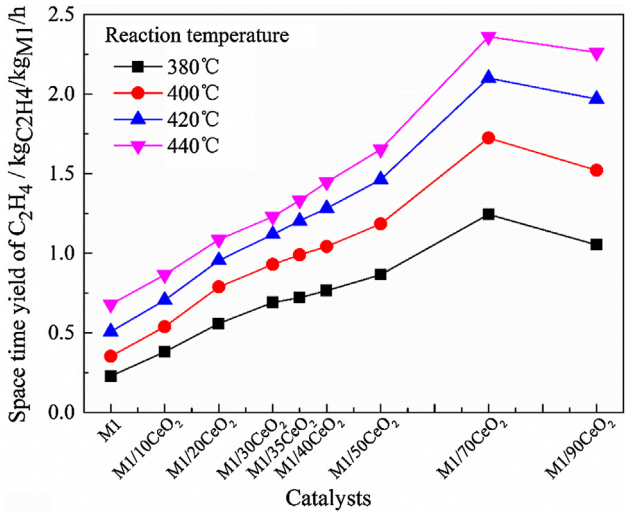

Fig. 6. Space time yield of ethylene as a function of CeO_2 content normalized by M1 content at different temperature.

where the maximum is found at CeO_2 addition of 30 wt.%. The space time yield of ethylene increases from 0.34 to 0.69 $kg_{C2H4}/kg_{cat}·h$ with the increase of CeO_2 addition from 0 to 30 wt.% and then decreases to 0.17 $kg_{C2H4}/kg_{cat}·h$ with the further increase of CeO_2 addition up to 90 wt.% at the contact time of 18.52 $g_{cat}·h/mol_{C2H6}$. For comparison, López Nieto et al. conducted ODHE on MoVNbTeOx system and reached a space time yield of 0.29 $kg_{C2H4}/kg_{cat}·h$ at 400 °C and C_2H_6:O_2:He molar ratio of 30:30:40 [39]. Meanwhile, the highest ethane conversion of 54.43% is achieved over the catalyst with a CeO_2 addition of 30 wt.% with ethylene selectivity of 83.9%, while phase-pure M1 attains only 24.20% ethane conversion under the same reaction conditions (Fig. 2). For the same M1 catalyst, when the amount of CeO_2 is added at 0–70 wt.%, the selectivity to ethylene drops with the increase of CeO_2 addition and ethane conversion. In contrast, a corresponding increase in selectivity to carbon oxides is observed as shown in Fig. 2. These results are consistent with the references [4,11,20,37]. Pure CeO_2 is not selective to ethylene, with ethane conversion of 6.9% and ethylene selectivity of 5.5% at 400 °C. Therefore, the lower selectivity of ethylene in M1/CeO_2 system is mainly caused by CeO_2 existence. The ethylene selectivity of M1/90CeO_2

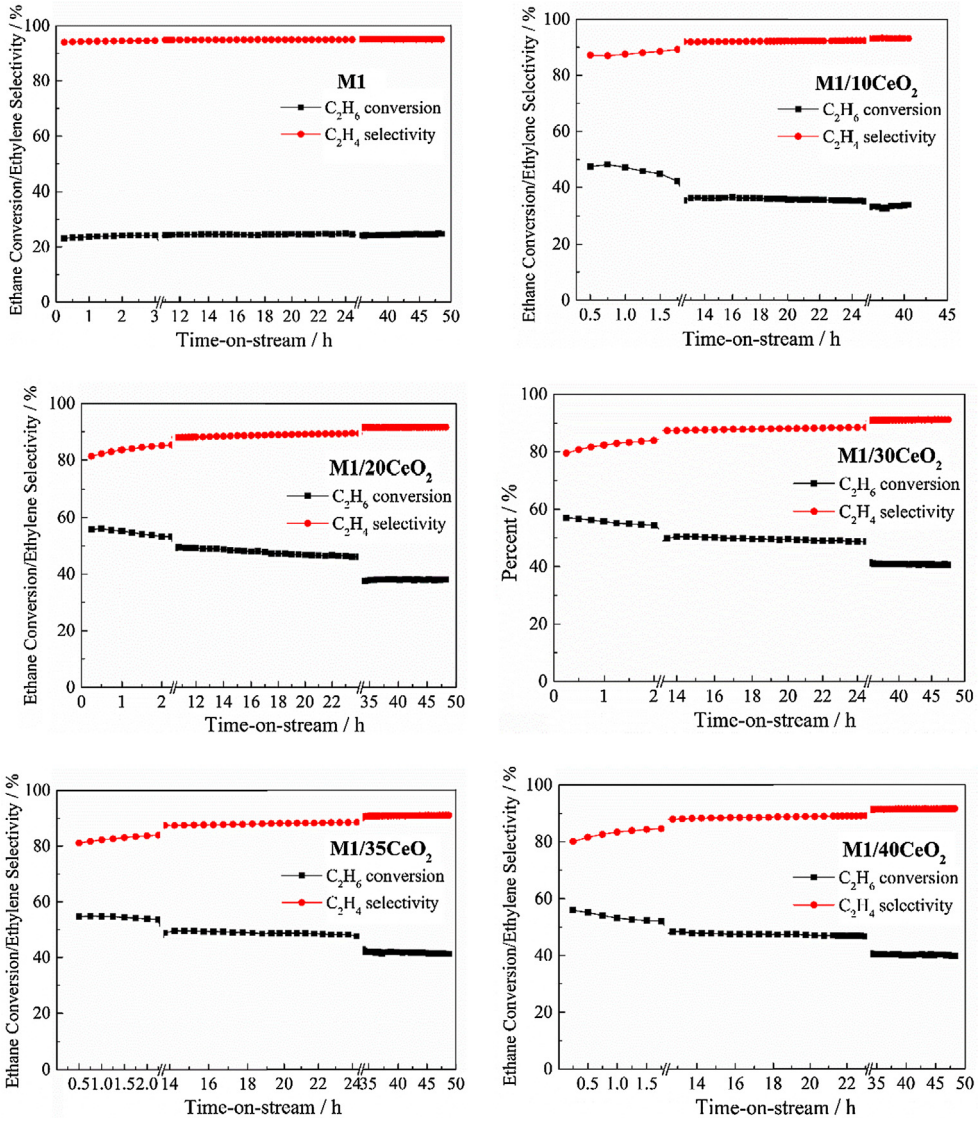

Fig. 7. Ethane conversion and ethylene selectivity as a function of reaction time for M1, CeO_2 and a series of M1/CeO_2 catalysts.

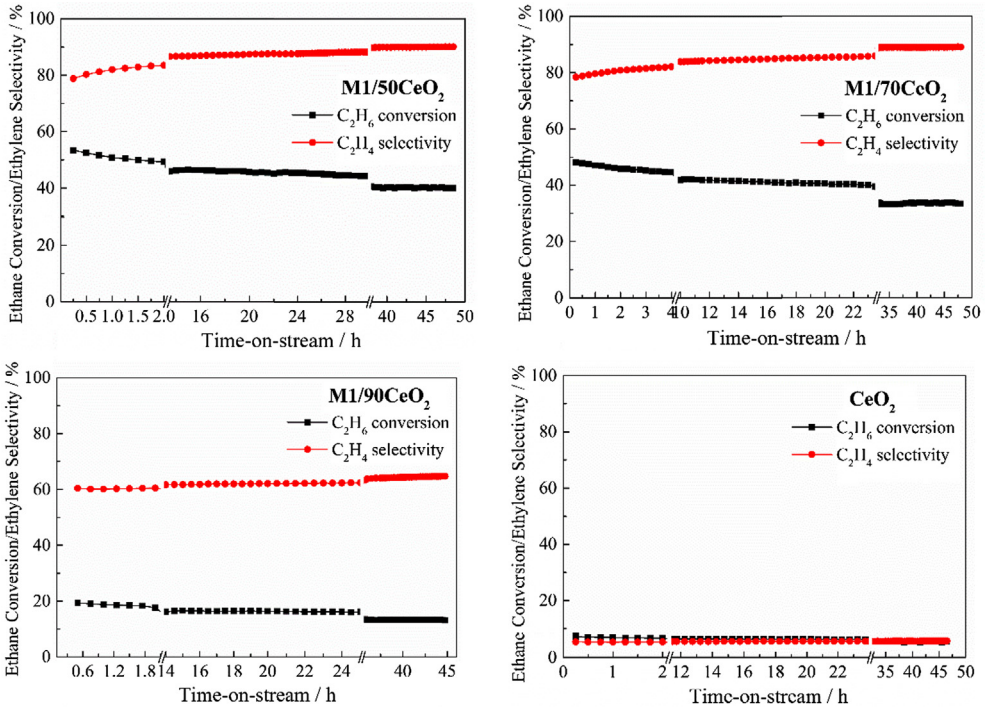

Fig. 7 (*continued*)

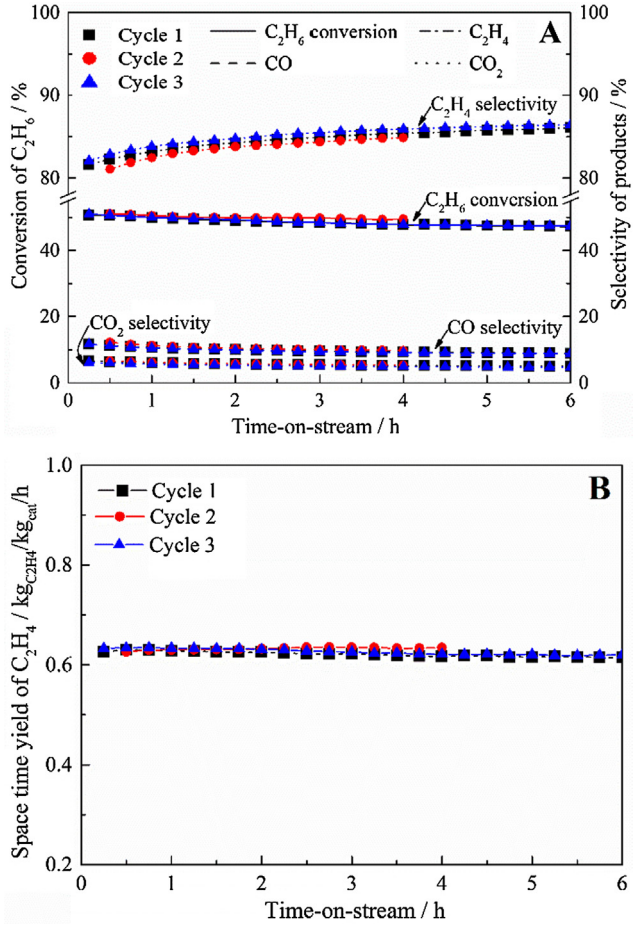

Fig. 8. C_2H_6 conversion, product selectivity (A) and space time yield (B) obtained after refreshment of M1/50CeO_2 in 3 cycles (reaction temperature of 400 °C,a contact time of 18.52 g_{cat}·h/mol_{C2H6}, C_2H_6/O_2/He molar ratio of 30/20/50 at the reactor inlet, time on stream of 4–6 h).

Table 2
Composition of the phase-pure M1 $MoVNbTeO_x/CeO_2$ catalysts.[a]

Catalysts	Mo-V-Nb-Te-Ce atomic ratio of bulk composition	Mo-V-Nb-Te-Ce atomic ratio of surface composition
M1	$MoV_{0.23}Nb_{0.25}Te_{0.11}$	$MoV_{0.15}Nb_{0.36}Te_{0.24}$
Used M1	$MoV_{0.23}Nb_{0.25}Te_{0.11}$	$MoV_{0.15}Nb_{0.33}Te_{0.23}$
M1/30CeO_2	$MoV_{0.23}Nb_{0.25}Te_{0.11}Ce_{0.44}$	$MoV_{0.21}Nb_{0.49}Te_{0.32}Ce_{0.95}$
Used M1/30CeO_2	$MoV_{0.23}Nb_{0.25}Te_{0.11}Ce_{0.44}$	$MoV_{0.20}Nb_{0.52}Te_{0.29}Ce_{0.93}$
M1/50CeO_2	$MoV_{0.23}Nb_{0.25}Te_{0.11}Ce_{1.04}$	$MoV_{0.19}Nb_{0.58}Te_{0.34}Ce_{1.89}$
Used M1/50CeO_2	$MoV_{0.23}Nb_{0.25}Te_{0.11}Ce_{1.04}$	$MoV_{0.21}Nb_{0.55}Te_{0.38}Ce_{1.71}$
Used M1/50CeO_2 for 6 h	$MoV_{0.23}Nb_{0.25}Te_{0.11}Ce_{1.04}$	$MoV_{0.21}Nb_{0.53}Te_{0.31}Ce_{1.84}$
Used M1/50CeO_2 for 6 h and refreshed by O_2 for 12 h	$MoV_{0.23}Nb_{0.25}Te_{0.11}Ce_{1.04}$	$MoV_{0.20}Nb_{0.52}Te_{0.34}Ce_{1.83}$

[a] Reaction condition of used catalysts: reaction temperature of 400 °C, contact time of 18.52 g_{cat}·h/mol_{C2H6}, C_2H_6/O_2/He molar ratio of 30/20/50 at the reactor inlet, time on stream of 50 h.

sample plummets compared to other samples, which presents a more similar property of pure CeO_2.

We should note that the catalyst weight for each reaction is the same, accordingly M1 content for ODHE decreases with the increase of CeO_2 addition. To justify the contribution of M1 itself, we normalize the space time yield by M1 content and the results are presented in Fig. 3. The normalized space time yield keeps increasing before CeO_2 addition reached 70%, and decreases when CeO_2 addition is 90%.

3.1.2. Effect of reaction temperature

Figs. 4–6 show the effect of reaction temperature (380–420 °C) on the catalytic performance of M1/ CeO_2 for ODHE at contact time of 18.52 g_{cat}·h/mol_{C2H6}.

As shown in Figs. 4–6, the reaction temperature has a significant effect on the activity of the catalysts. When the reaction temperature is ranged from 380 °C to 440 °C, the conversion of ethane increases linearly with the increase of reaction temperature [40]. The normalized space time yield also shows a similar trend as above.

3.1.3. Catalyst stability

Stability is an extremely important property that may determine whether a catalyst has the potential for industrial application or not. Time-on-stream experiments are carried out in order to study the stability of the above-mentioned catalysts. As presented in Fig. 7, the phase-pure M1 catalyst and the pure CeO_2 exhibit stable catalytic performance in 50 h time-on-stream tests. However, the ethane conversions for all the M1/CeO_2 catalysts decrease at different levels with the progress of the reaction time and the ethylene selectivity has a corresponding increase.

Generally, oxidative dehydrogenation process based on vanadium-based catalyst is described by Mars and van Krevelen (MvK) mechanism: alkane molecules react with lattice oxygen of the catalyst to produce alkene molecules and carbon oxides; the gas phase oxygen replenishes the lattice oxygen by the re-oxidation of the catalyst [41,42]. Considering pure M1 is quite stable during reaction, we suppose that the conversion decrease is not from structure damage but from the loss of lattice oxygen: the oxygen in the reactant gas would not be sufficient to supplement the loss of lattice oxygen in the catalytic materials. Therefore, we have the plan to perform the following refreshment test.

3.1.4. Catalyst refreshment

Since the series of M1/CeO_2 catalysts show the similar catalytic performances in ODHE reaction, M1/50CeO_2 is chosen as a representative to test the reproducibility by refreshment after usage. A used catalyst is refreshed by feeding 10 ml/min pure oxygen in situ at 400 °C for 12 h, and then pure helium is switched on to replace residual oxygen in the reactor before feeding the reactant gases (i.e., a C_2H_6/O_2/He molar ratio of 30/20/50 at 400 °C and a contact time of 18.52 g_{cat}·h/mol_{C2H6}). Fig. 8 shows the comparison of the obtained C_2H_6 conversion, product selectivity and space time yield. Overall, C_2H_6 conversion and product selectivity are stable in the three cycles of refreshment with similar space time yields, which indicates a good reproducibility of M1/50CeO_2 catalyst and a good repeatability of the experimental results. It could be deduced that after a long period of reaction, the decrease of ethane conversion is due to the loss of lattice oxygen, while the in-situ supplement of oxygen could make M1/CeO_2 system re-gain similar activity as fresh catalyst.

3.2. Catalyst characterization

3.2.1. Elemental composition and textural properties

The bulk composition characterized by ICP-OES and surface composition characterized by XPS of phase-pure M1 $MoVNbTeO_x$ and M1/CeO_2 catalysts are provided in Table 2. For the bulk composition, there is little difference in terms of the chemical composition compared to that of the M1 phase reported in the literature [11,14,36,43,44]. It is reported that the metal content of phase-pure M1 is not restricted to a specific molar ratio of the metals in the structure, but covers the region of metal content for phase-pure M1 in the quaternary phase diagram [45]. In this work, all the pure phase M1 and M1/CeO_2 catalysts are consistent with the mentioned properties. The addition of CeO_2 to phase-pure M1 has no effect on the chemical composition. XPS surface composition analysis is semi-quantitative. We could see that the surface composition is quite different from bulk composition. Molybdenum seems to decrease a little after CeO_2 addition. While the catalyst before and after reaction has similar surface composition, which indicates the stability of this catalyst system.

The BET measurements of samples are listed in Table 3. The specific surface area and pore volume of phase-pure M1 catalyst are relatively low, but increase considerably upon loading of CeO_2. This increase can be attributed to the addition of CeO_2-gel as starting compound for CeO_2, which is much larger than the addition of other elements to M1 phase [15,46]. The decomposition during calcination of precursors with organic nature causes a more porous structure than M1 catalyst. The previous works have proved that surface area is not related to catalytic performance [11,20,47]. After refreshment, the surface area is similar to the used catalyst, while the catalytic performance is higher, which also proves this.

3.2.2. X-ray diffraction (XRD)

Fig. 9 shows the X-ray diffraction patterns of the catalysts. Characteristic peaks of M1(ICSD 55097) at 2θ = 6.6°, 7.7°, 8.9°, 10.7°, 22.1°, 27.2°, 29.2°, 35.48° [48] are observed in all samples except the pure CeO_2. The presence of CeO_2 diffraction signals, located at 2θ = 28.6°, 33.1°, 56.4°, 59.1°, 69.5°(JCPDS 43-1002), indicates the presence of CeO_2 to the surface of M1 material. No other crystalline peaks are detected in all the samples, which can be

Table 3
Textural characterization of the phase-pure M1 $MoVNbTeO_x$/CeO_2 catalysts.

Catalysts	Specific surface area m^2/g	Pore Volume cc/g
M1	16	0.056
Used M1	12	0.052
M1/10CeO_2	39	0.166
Used M1/10CeO_2	14	0.080
M1/30CeO_2	42	0.133
Used M1/30CeO_2	21	0.095
M1/50CeO_2	32	0.081
Used M1/50CeO_2 for 6 h	30	0.076
Used M1/50CeO_2 for 6 h and refreshed by O_2 for 12 h	29	0.073
Used M1/50CeO_2	25	0.068
CeO_2	30	0.028
Used CeO_2	28	0.024

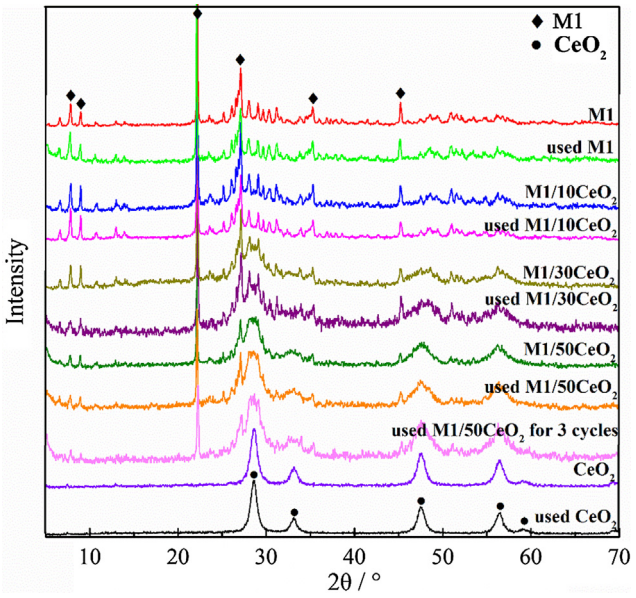

Fig. 9. XRD patterns of the catalysts (reaction condition of used catalysts: reaction temperature of 400 °C, contact time of 18.52 g_{cat}·h/mol_{C2H6}, C_2H_6/O_2/He molar ratio of 30/20/50 at the reactor inlet, time on stream of 50 h).

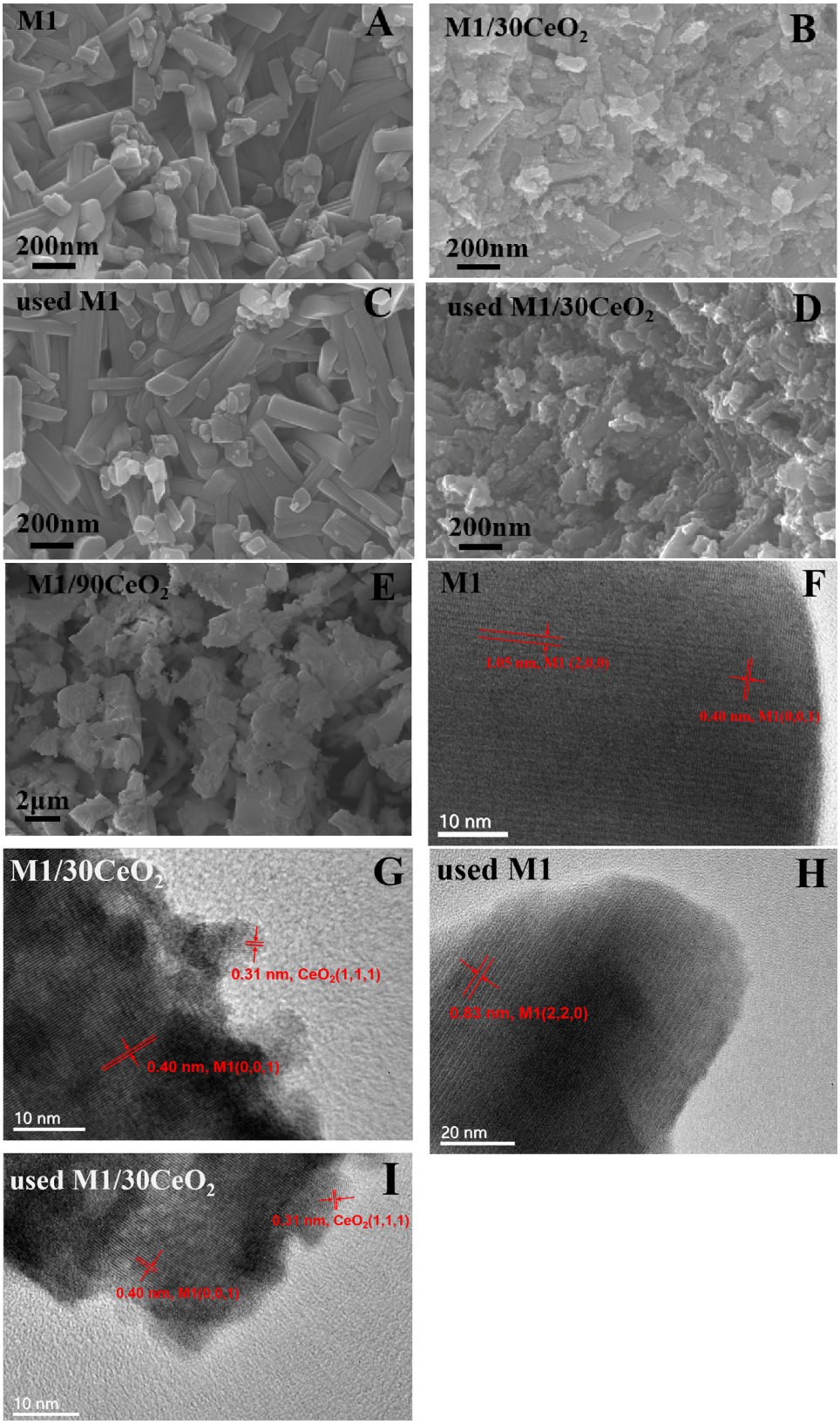

Fig. 10. SEM images (A-E) and TEM images (F-I) of fresh and used catalysts (M1, M1/30CeO_2, M1/90CeO_2, reaction condition of used catalysts: reaction temperature of 400 °C, a contact time of 18.52 g_{cat}·h/mol_{C2H6}, C_2H_6/O_2/He molar ratio of 30/20/50 at the reactor inlet, time on stream of 50 h).

attributed to the purification of $MoVNbTeO_x$ materials by HNO_3 solution. The full width at half height of the peaks decreases as the amount of CeO_2 increases, indicating an increase in the size of the crystalline domain of the ceria phase [49]. As presented in Fig. 9, apparently, no significant change can be observed in XRD patterns of fresh catalyst, used catalysts and the catalyst used for 3 cycles in the refreshment test, which illustrates a relative stable crystal structure during reaction.

3.2.3. Catalyst morphology

The surface morphology of the synthesized materials is examined by SEM. Micrographs of the fresh M1 catalyst and M1/CeO_2 catalysts with different CeO_2 contents, together with the corresponding used catalyst, are presented in Fig. 10(A–E). Electronic images of the catalysts used before and after refreshment is also presented in Fig. 10(F–I). It is obvious that the rod-like M1 phase crystal has an average width of ~100 nm and an average length of ~200 nm, just as reported in the literature [11]. A bronzelike channel structure grows along the (0 0 1) direction and a rodlike crystal morphology finally forms in which the (0 0 1) planes are perpendicular to the axis length of the rod in the M1 phase [50]. The SEM images display a good dispersion of homogeneous CeO_2 particles on the surface of fresh M1/30CeO_2 and M1/50CeO_2. It can be seen that the more CeO_2 content, the more CeO_2 particles on the surface of the catalysts, which is consistent with the result of surface areas detected by the previous characterization techniques (Table 3). However, for the M1/90CeO_2 catalyst, the surface is covered by CeO_2 and almost no M1 could be observed, which may result in the decrease of space time yield to CeO_2 content normalized by M1 content, as displayed in Figs. 3 and 6. In the TEM images, two different crystals can be observed in the M1/CeO_2 catalysts, which represent M1 and CeO_2 crystal, respectively. The morphology of fresh and used catalysts (Fig. 11), the M1/50CeO_2 catalyst before and after 3 cycles of refreshment, has almost no change compared to each other, which indicates the structural stability of the M1/CeO_2 catalysts in such long time-on-stream experiments and refreshment test.

3.2.4. X-ray photoelectron spectroscopy analysis (XPS)

XPS spectra of key elements in fresh and used phase-pure M1 and M1/CeO_2 catalysts are measured to investigate the change of element valence states on the catalyst surface with the addition of different CeO_2 content (Fig. 12). The binding energy data of the reference materials are obtained from the NIST X-ray Photoelectron Spectroscopy Database.

As shown in Fig. 12(A, C, D), the binding energy of Mo 3d (232.9 ± 0.2 eV), Nb 3d (207.2 ± 0.2 eV), Te 3d (576.3 ± 0.2 eV) is the same as reported, corresponding to valence states of Mo^{6+}, $Nb^{5+}$and Te^{4+}, respectively [11,38]. These results suggest that the introduction of CeO_2 has little influence on the valence states of these three elements in M1/CeO_2 catalysts. Besides, there is no effect on the change of valence states in those elements in the time-on-stream experiments for 50 h.

Fig. 12(B) and (E) show the XPS spectra of vanadium and cerium of the fresh and used catalyst samples (M1, M1/30CeO_2, M1/50CeO_2 and CeO_2). Table 4 shows the ratio variations of vanadium and cerium valence states of catalysts mentioned above. As illustrated in Fig. 12(B), the V 2p3/2 peak of catalysts could be fitted into two components at 517.10 ± 0.05 eV and 516.20 ± 0.05 eV, with FWHM of both peaks as 1.3 ± 0.1 eV., representing V^{4+} and V^{5+} species, respectively [51,52]. The Ce $3d_{3/2,\ 5/2}$ spectra are composed of two multiplets (v and u) corresponding to the spin-orbit split $3d_{5/2}$ and $3d_{3/2}$ core holes. The highest binding energy peaks, u'' and v'' respectively locating at about 916.5 and 898.4 ± 0.1 eV are the result of a Ce $3d^94f^0$ final state. The satellite peak u'' associated to the Ce $3d_{3/2}$ is characteristic of the presence of tetravalent Ce (Ce^{4+} ions) in Ce compounds. The lowest binding energy states u^0, v^0, v', u' respectively located at 900.9, 882.2, 907.6 and 889.4 ± 0.1 eV are the result of Ce $3d^94f^2$ and Ce $3d^94f^1$ final states, which is in good agreement with references [53–55]. The XPS characterization indicates that the Ce^{3+} and Ce^{4+} species can be fitted to distinct line shapes corresponding to various final states: Ce (III) = v + v'' + u and Ce(IV) = v^0 + v' + u^0 + u' + u''. The calculated results can be seen in Table 4.

As listed in Table 4, a greater amount of V^{5+} can be achieved in the fresh Ce-containing catalyst surface than that on the Ce-free catalyst surface. In addition, the more the CeO_2 content is introduced, the more the ratio of V^{5+}/ V^{4+} increases. At the same time, the ratio of Ce^{3+}/Ce^{4+} goes up accordingly. This phenomenon implies that the increase of V^{5+} abundance on the catalyst surface is benefitted from the transition of $Ce^{4+}\rightarrow Ce^{3+}$ in the solid phase of M1/CeO_2 catalysts. Compared to the pure phase-M1 catalyst, the catalytic performance of M1/CeO_2 catalysts is enhanced effectively, resulting from the increase of V^{5+} abundance on the catalyst surface. This can be demonstrated by the experimental results in Sections 3.1.1 and 3.1.2.

For the refreshment test, we can see after the in-situ oxygen treatment, V^{5+}/V^{4+} ratio of refreshed catalyst recovered, meaning

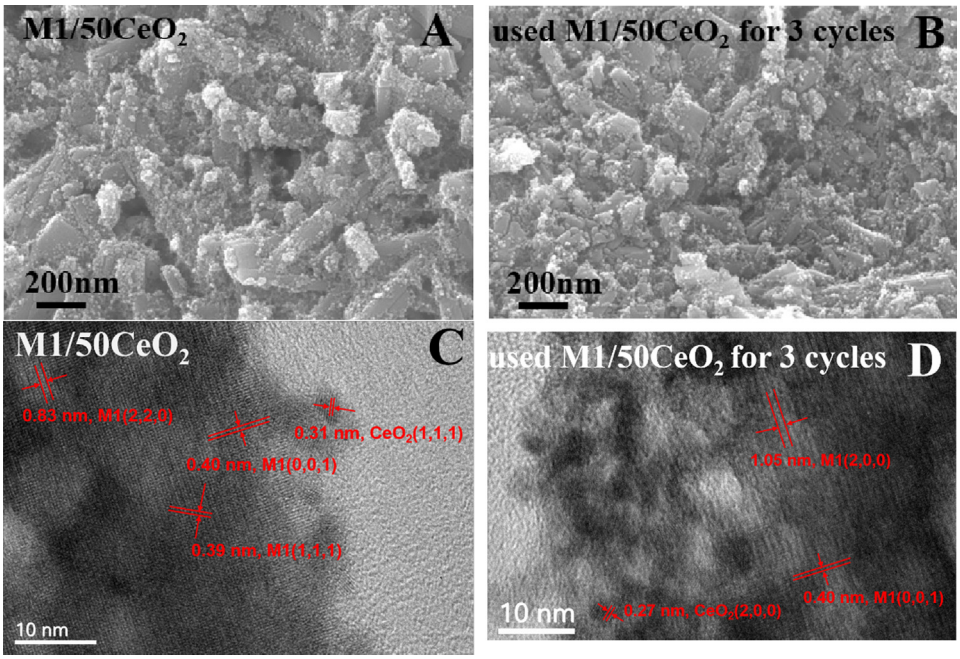

Fig. 11. Characterization of XRD, SEM and TEM on the fresh and used M1/50CeO_2 catalyst after 3 cycles of refreshment.

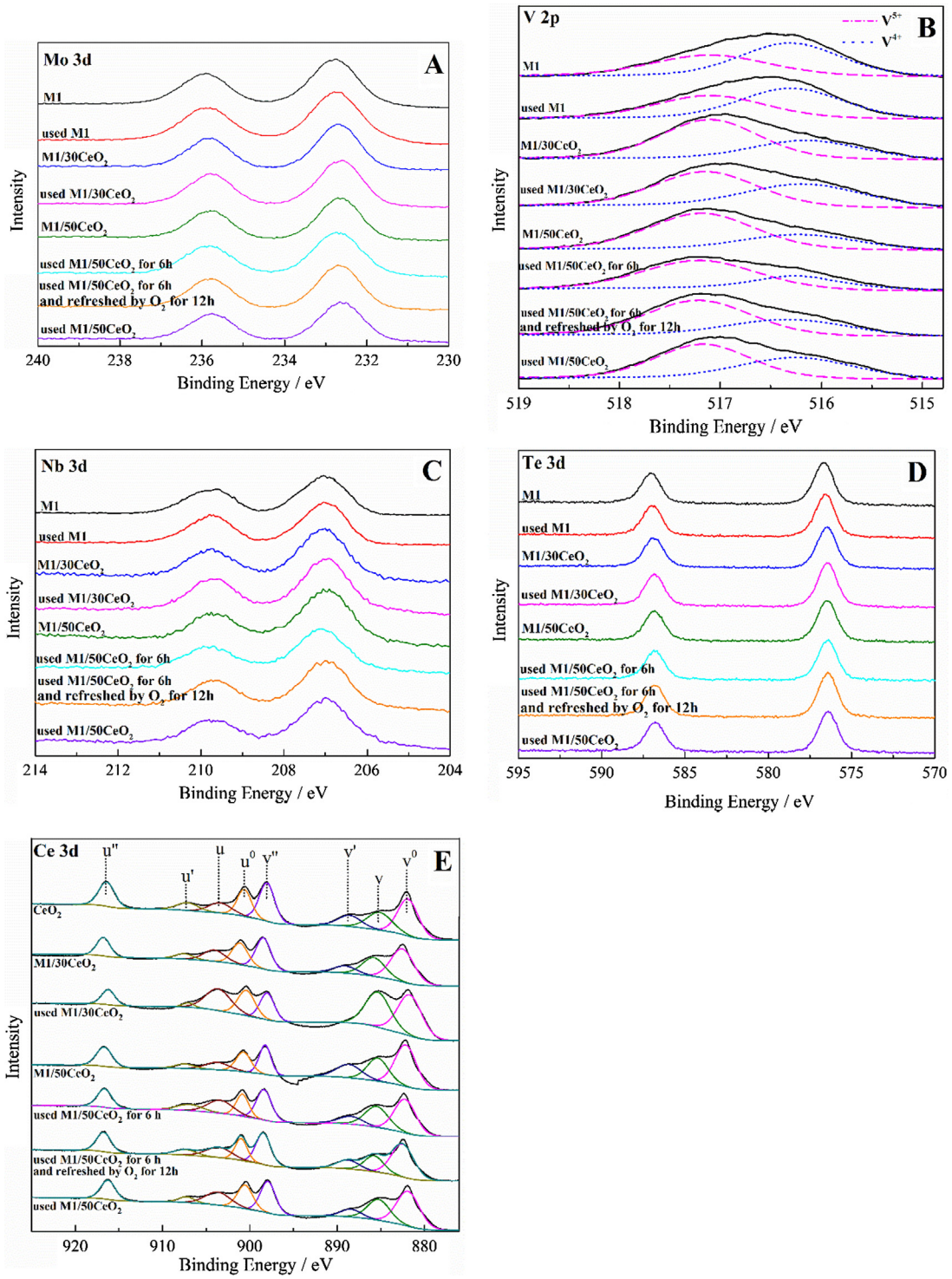

Fig. 12. XPS spectra of fresh and used catalysts (M1, M1/30CeO_2, M1/50CeO_2). A: Mo 3d; B: V 2P; C: Nb 3d; D: Te 3d; E: Ce 3d. Reaction condition of used catalysts: reaction temperature of 400 °C,a contact time of 18.52 g_{cat}·h/mol_{C2H6}, C_2H_6/O_2/He molar ratio of 30/20/50 at the reactor inlet, time on stream of 50 h.

that the oxygen supplement can make up the lattice oxygen loss during reaction.

Assuming that surface V^{5+} is the only active site for ethane conversion, we thus define the turnover frequency of this system as the converted ethane molecules per second over a single V^{5+} site. The calculated TOFs for these catalyst are listed in Table 5 using BET measurement results, ethane conversion data, XPS deconvolution results and lattice parameter of M1 [56,57]. We can see that adding CeO_2 into this catalyst system obviously increases the turn-over frequency. It could be inferred that the ability of oxygen transfer from Ce^{4+} to V^{4+} is easier than gas phase transmission. The transformation between V^{5+} and V^{4+} occurs dynamically during the reaction [44], although the TOF calculation assumes that the amount of active site (i.e., V^{5+}) is constant. For pure M1, V^{5+} sites oxidize ethane and then are re-oxidized mainly by gas phase oxygen. In contrast, with the presence of CeO_2, the re-oxidation of V^{4+} to V^{5+} is dominated by an easier way (i.e., by Ce^{4+}), leading to an increase of the turn-over frequency for this process. This

Table 4
Ratios of vanadium and cerium valence states of fresh and used catalysts[a] in ODHE process.

Catalysts	V^{5+}/V^{4+}	Ce^{3+}/Ce^{4+}
M1	0.75	–
Used M1	0.82	–
M1/30CeO_2	1.84	0.70
Used M1/30CeO_2	1.27	1.07
M1/50CeO_2	2.13	0.53
Used M1/50CeO_2 for 6 h	1.80	0.70
Used M1/50CeO_2 for 6 h and refreshed by O_2 for 12 h	1.95	0.69
Used M1/50CeO_2	1.31	0.74
CeO_2	–	0.65

[a] Reaction condition of used catalysts: reaction temperature of 400 °C, contact time of 18.52 g_{cat}·h/mol_{C2H6}, C_2H_6/O_2/He molar ratio of 30/20/50 at the reactor inlet, time on stream of 50 h.

Table 5
TOF estimates for M1 and M1/CeO_2 catalysts.

Catalysts	M1	M1/30CeO_2	M1/50CeO_2
TOF/mol_{C2H6}.mol^{-1}_{V5+}·s^{-1}	0.29	0.61	0.75

phenomenon was also observed by Wang et al. [58], that is, cerium helped the re-oxidation of molybdenum and vanadium. In addition, as the supplement of oxygen from gas phase to solid phase cannot meet the lattice oxygen loss during reaction, the lattice oxygen in the whole system decreases with time, which explains the decrease of ethane conversion during stability testing, and is consistent with the XPS analysis.

4. Conclusions

A series of M1/CeO_2 catalysts have been prepared and evaluated in ODHE process at different contact times and reaction temperatures. It is found that phase-pure M1 with 30 wt.% CeO_2 catalyst has the best catalytic performance. Although the ethane conversion decreases with reaction time, the activity could be re-gained after refreshment by supplying oxygen in situ. It is shown that the increase of V^{5+} amount is one of the dominant factors for higher ethane conversion. In addition, by estimating the TOFs for this complex system based on experiment results and characterization results, we found that the existence of Ce^{4+} makes the re-oxidation of V^{4+} process easier and hence the turn-over frequency is increased. This also explains the loss of lattice oxygen in M1/CeO_2 catalyst during ODHE reaction. The used catalyst after 3 cycles of refreshment maintains stable in crystal structure and surface morphology. The results encourage further research on the better understanding of the catalytic mechanism and performance manipulation (i.e., activity, selectivity and stability) of M1/CeO_2 catalysts during the application in ODHE process.

Acknowledgment

This work is financially supported by the National Natural Science Foundation of China (21776156).

References

[1] C.A. Gärtner, A.C. Van Veen, J.A. Lercher, Oxidative dehydrogenation of ethane: common principles and mechanistic aspects, ChemCatChem 5 (2013) 3196.
[2] B. Solsona, F. Ivars, A. Dejoz, P. Concepción, M.I. Vázquez, J.M. López Nieto, Supported Ni-W-O mixed oxides as selective catalysts for the oxidative dehydrogenation of ethane, Top. Catal. 52 (2009) 751.
[3] G. Centi, F. Cavani, F. Trifirò, Selective oxidation by heterogeneous catalysis, Fundam. Appl. Catal. 132 (2001) 1252.
[4] P. Botella, E. García-González, A. Dejoz, J.M. López Nieto, M.I. Vázquez, J. González-Calbet, Selective oxidative dehydrogenation of ethane on MoVTeNbO mixed metal oxide catalysts, J. Catal. 225 (2004) 428.
[5] J.M.L. Nieto, The selective oxidative activation of light alkanes. From supported vanadia to multicomponent bulk V-containing catalysts, Top. Catal. 41 (2006) 3.
[6] P. Botella, A. Dejoz, J.M. López Nieto, P. Concepción, M.I. Vázquez, Selective oxidative dehydrogenation of ethane over MoVSbO mixed oxide catalysts, Appl. Catal. A-Gen. 298 (2006) 16.
[7] X. Zhang, J. Liu, Y. Jing, Y. Xie, Support effects on the catalytic behavior of NiO/Al_2O_3 for oxidative dehydrogenation of ethane to ethylene, Appl. Catal. A-Gen. 240 (2003) 143.
[8] E. Heracleous, A.F. Lee, K. Wilson, A.A. Lemonidou, Investigation of Ni-based alumina-supported catalysts for the oxidative dehydrogenation of ethane to ethylene: structural characterization and reactivity studies, J. Catal. 231 (2005) 159.
[9] E. Heracleous, A.A. Lemonidou, Ni-Nb-O mixed oxides as highly active and selective catalysts for ethene production via ethane oxidative dehydrogenation. Part I: characterization and catalytic performance, J. Catal. 237 (2006) 162.
[10] E. Heracleous, A.A. Lemonidou, Ni-Nb-O mixed oxides as highly active and selective catalysts for ethene production via ethane oxidative dehydrogenation. Part II: mechanistic aspects and kinetic modeling, J. Catal. 237 (2006) 175.
[11] B.B. Chu, A. Hang, J.J. Schouten, Y. Cheng, A self-redox phase-pure M1 MoVNbTeO$_x$/CeO_2 nanocomposite as a highly active catalyst on oxidative dehydrogenation of ethane, J. Catal. 329 (2015).
[12] Y. Zhu, J. Eric, P.V. Sushko, K. Libor, M. Daniel, S.S. Maricruz, J.A. Lercher, N.D. Browning, Revealing the working active sites of M1 phase for ethane oxidation, Microsc. Microanal. 22 (2016) 790.
[13] G.Y. Popova, T.V. Andrushkevich, Y.A. Chesalov, L.M. Plyasova, L.S. Dovlitova, E. V. Ischenko, G.I. Aleshina, M.I. Khramov, Formation of active phases in MoVTeNb oxide catalysts for ammoxidation of propane, Catal. Today 144 (2009) 312.
[14] T.T. Nguyen, M. Aouine, J.M.M. Millet, Optimizing the efficiency of MoVTeNbO catalysts for ethane oxidative dehydrogenation to ethylene, Catal. Commun. 21 (2012) 22.
[15] E.V. Ishchenko, T.Y. Kardash, R.V. Gulyaev, A.V. Ishchenko, V.I. Sobolev, V.M. Bondareva, Effect of K and Bi doping on the M1 phase in MoVTeNbO catalysts for ethane oxidative conversion to ethylene, Appl. Catal. A-Gen. 514 (2016) 1.
[16] J.M. Oliver, J.M. López Nieto, P. Botella, A. Mifsud, The effect of pH on structural and catalytic properties of MoVTeNbO catalysts, Appl. Catal. A-Gen. 257 (2004) 67.
[17] K. Asakura, K. Nakatani, T. Kubota, Y. Iwasawa, Characterization and kinetic studies on the highly active ammoxidation catalyst MoVNbTeOx, J. Catal. 194 (2000) 309.
[18] E. Sadovskaya, V. Goncharov, G. Popova, E. Ishchenko, D. Frolov, A. Fedorova, T. Andrushkevich, Mo-V-Te-Nb oxide catalysts: reactivity of different oxygen species in partial and deep oxidation, J. Mol. Catal. A: Chem. 392 (2014) 61.
[19] P. Botella, J.M. López Nieto, B. Solsona, A. Mifsud, F. Márquez, The preparation, characterization, and catalytic behavior of MoVTeNbO catalysts prepared by hydrothermal synthesis, J. Catal. 209 (2002) 445.
[20] B. Chu, L. Truter, T.A. Nijhuis, Y. Cheng, Performance of phase-pure M1 MoVNbTeOx catalysts by hydrothermal synthesis with different post-treatments for the oxidative dehydrogenation of ethane, Appl. Catal. A-Gen. 498 (2015) 99.
[21] T. Ushikubo, K. Oshima, A. Kayou, M. Hatano, Ammoxidation of propane over Mo-V-Nb-Te mixed oxide catalysts, in: C. Li, Q. Xin (Eds.), Stud. Surf. Sci. Catal., Elsevier, 1997, p. 473.
[22] A. Celaya Sanfiz, T.W. Hansen, A. Sakthivel, A. Trunschke, R. Schlögl, A. Knoester, H.H. Brongersma, M.H. Looi, S.B.A. Hamid, How important is the (001) plane of M1 for selective oxidation of propane to acrylic acid?, J Catal. 258 (2008) 35.
[23] R.K. Grasselli, D.J. Buttrey, P. DeSanto, J.D. Burrington, C.G. Lugmair, A.F. Volpe, T. Weingand, Active centers in Mo-V-Nb-Te-O_x (amm) oxidation catalysts, Catal. Today 91–92 (2004) 251.
[24] X. Li, D.J. Buttrey, D.A. Blom, T. Vogt, Improvement of the structural model for the M1 phase Mo-V-Nb-Te-O propane (amm) oxidation catalyst, Top. Catal. 54 (2011) 614.
[25] B. Deniau, T.T. Nguyen, P. Delichere, O. Safonova, J.M.M. Millet, Redox state dynamics at the surface of MoVTe(Sb)NbO M1 phase in selective oxidation of light alkanes, Top. Catal. 56 (2013) 1952.
[26] Q. Xie, L. Chen, W. Weng, H. Wan, Preparation of MoVTe(Sb)Nb mixed oxide catalysts using a slurry method for selective oxidative dehydrogenation of ethane, J. Mol. Catal. A: Chem. 240 (2005) 191.
[27] M.M. Bhasin, Is true ethane oxydehydrogenation feasible?, Top Catal. 23 (2003) 145.
[28] D. Sanfilippo, I. Miracca, Dehydrogenation of paraffins: synergies between catalyst design and reactor engineering, Catal. Today 111 (2006) 133.
[29] F. Cavani, N. Ballarini, A. Cericola, Oxidative dehydrogenation of ethane and propane: how far from commercial implementation?, Catal Today 127 (2007) 113.
[30] C.A. Gärtner, A.C. Van Veen, J.A. Lercher, Oxidative dehydrogenation of ethane: common principles and mechanistic aspects, ChemCatChem 5 (2014) 3196.
[31] B. Solsona, M.I. Vázquez, F. Ivars, A. Dejoz, P. Concepción, J.M. López Nieto, Selective oxidation of propane and ethane on diluted Mo-V-Nb-Te mixed-oxide catalysts, J. Catal. 252 (2007) 271.

[32] B. Solsona, P. Concepción, S. Hernández, B. Demicol, J.M.L. Nieto, Oxidative dehydrogenation of ethane over NiO-CeO_2 mixed oxides catalysts, Catal. Today 180 (2012) 51.
[33] Y. Li, Z. Wei, F. Gao, L. Kovarik, C.H.F. Peden, Y. Wang, Effects of CeO_2 support facets on VO_x/CeO_2 catalysts in oxidative dehydrogenation of methanol, J. Catal. 315 (2014) 15.
[34] J. Fan, X. Wu, X. Wu, Q. Liang, R. Ran, D. Weng, Thermal ageing of Pt on low-surface-area CeO_2-ZrO_2-La_2O_3 mixed oxides: effect on the OSC performance, Appl. Catal., B 81 (2008) 38.
[35] G. Raju, B.M. Reddy, S.-E. Park, CO2 promoted oxidative dehydrogenation of n-butane over VO_x/MO_2-ZrO_2 (M=Ce or Ti) catalysts, J. CO_2 Utilization 5 (2014) 41.
[36] A. Celaya Sanfiz, T.W. Hansen, F. Girgsdies, O. Timpe, E. Rödel, T. Ressler, A. Trunschke, R. Schlögl, Preparation of Phase-Pure M1 MoVTeNb Oxide Catalysts by Hydrothermal Synthesis-Influence of Reaction Parameters on Structure and Morphology, Top. Catal. 50 (2008) 19.
[37] B. Chu, H. An, X. Chen, Y. Cheng, Phase-pure M1 MoVNbTeOx catalysts with tunable particle size for oxidative dehydrogenation of ethane, Appl. Catal. A-Gen. 524 (2016) 56.
[38] B. Solsona, M.I. Vázquez, F. Ivars, A. Dejoz, P. Concepción, J.M.L. Nieto, Selective oxidation of propane and ethane on diluted Mo-V-Nb-Te mixed-oxide catalysts, J. Catal. 252 (2007) 271.
[39] J.M. López Nieto, P. Botella, M.I. Vázquez, A. Dejoz, The selective oxidative dehydrogenation of ethane over hydrothermally synthesised MoVTeNb catalysts, Chem. Commun. 8 (2002) 1906.
[40] M.V. Martínez-Huerta, X. Gao, H. Tian, I.E. Wachs, J.L.G. Fierro, M.A. Bañares, Oxidative dehydrogenation of ethane to ethylene over alumina-supported vanadium oxide catalysts: relationship between molecular structures and chemical reactivity, Catal. Today 118 (2006) 279.
[41] P. Mars, D.W. van Krevelen, Oxidations carried out by means of vanadium oxide catalysts, Chem. Eng. Sci. 3 (1954) 41.
[42] D. Linke, D. Wolf, M. Baerns, S. Zeyß, U. Dingerdissen, Catalytic Partial Oxidation of Ethane to Acetic Acid over $Mo_1V_{0.25}Nb_{0.12}Pd_{0.0005}O_x$: II. Kinetic Modelling, J. Catal. 205 (2002) 32.
[43] T.T. Nguyen, L. Burel, D.L. Nguyen, C. Pham-Huu, J.M.M. Millet, Catalytic performance of MoVTeNbO catalyst supported on SiC foam in oxidative dehydrogenation of ethane and ammoxidation of propane, Appl. Catal. A-Gen. 433–434 (2012) 41.
[44] M. Hävecker, S. Wrabetz, J. Kröhnert, L.-I. Csepei, R. Naumann d'Alnoncourt, Y. V. Kolen'ko, F. Girgsdies, R. Schlögl, A. Trunschke, Surface chemistry of phase-pure M1 MoVTeNb oxide during operation in selective oxidation of propane to acrylic acid, J. Catal. 285 (2012) 48.
[45] A.C. Sanfiz, T.W. Hansen, D. Teschner, P. Schnörch, F. Girgsdies, A. Trunschke, R. Schlögl, H.L. Ming, S.B.A. Hamid, Dynamics of the MoVTeNb oxide M1 phase in propane oxidation, J. Phys. Chem. 114 (2010) 1912.
[46] T.V. Andrushkevich, G.Y. Popova, Y.A. Chesalov, E.V. Ischenko, M.I. Khramov, V. V. Kaichev, Propane ammoxidation on Bi promoted MoVTeNbOx oxide catalysts: effect of reaction mixture composition, Appl. Catal. A-Gen. 506 (2015) 109.
[47] Y.V. Kolen'Ko, W. Zhang, R.N. D'Alnoncourt, F. Girgsdies, T.W. Hansen, T. Wolfram, R. Schlögl, A. Trunschke, Synthesis of MoVTeNb oxide catalysts with tunable particle dimensions, Chemcatchem 3 (2011) 1597.
[48] P. Botella, E. Garcia-Gonzalez, J.M.L. Nieto, J.M. Gonzalez-Calbet, MoVTeNbO multifunctional catalysts: correlation between constituent crystalline phases and catalytic performance, Cheminform 7 (2005) 507.
[49] J.P. Bortolozzi, T. Weiss, L.B. Gutierrez, M.A. Ulla, Comparison of Ni and Ni-Ce/Al_2O_3 catalysts in granulated and structured forms: their possible use in the oxidative dehydrogenation of ethane reaction, Chem. Eng. J. 246 (2014) 343.
[50] P. DeSanto Jr, D.J. Buttrey, R.K. Grasselli, C.G. Lugmair, A.F. Volpe, B.H. Toby, T. Vogt, Structural characterization of the orthorhombic phase M1 in MoVNbTeO propane ammoxidation catalyst, Top. Catal. 23 (2003) 23.
[51] J. Guan, S. Wu, H. Wang, S. Jing, G. Wang, K. Zhen, Q. Kan, Synthesis and characterization of MoVTeCeO catalysts and their catalytic performance for selective oxidation of isobutane and isobutylene, J. Catal. 251 (2007) 354.
[52] M. Demeter, M. Neumann, W. Reichelt, Mixed-valence vanadium oxides studied by XPS, Surf. Sci. 454 (2000) 41.
[53] E. Bêche, P. Charvin, D. Perarnau, S. Abanades, G. Flamant, Ce 3d XPS investigation of cerium oxides and mixed cerium oxide ($Ce_xTi_yO_z$), Surf. Interface Anal. 40 (2008) 264.
[54] F.ç. Larachi, J. Pierre, A. Adnot, A. Bernis, Ce 3d XPS study of composite $Ce_xMn_{1-x}O_{2-y}$ wet oxidation catalysts, Appl. Surf. Sci. 195 (2002) 236.
[55] J. Guan, S. Wu, H. Wang, S. Jing, G. Wang, K. Zhen, Q. Kan, Synthesis and characterization of MoVTeCeO catalysts and their catalytic performance for selective oxidation of isobutane and isobutylene, Int. J. Chem. Reactor Eng. 251 (2014) 354.
[56] P. Desanto Jr, D.J. Buttrey, R.K. Grasselli, C.G. Lugmair, A.F. Volpe Jr, B.H. Toby, T. Vogt, Structural aspects of the M1 and M2 phases in MoVNbTeO propane ammoxidation catalysts, Z. Kristallogr.-Cryst. Mater. 219 (2004) 152.
[57] W.D. Pyrz, D.A. Blom, T. Vogt, D.J. Buttrey, Direct imaging of the MoVTeNbO M1 phase using an aberration-corrected high-resolution scanning transmission electron microscope, Angew. Chem. Int. Ed. 47 (2008) 2788.
[58] G. Wang, Y. Guo, G. Lu, Promotional effect of cerium on Mo-V-Te-Nb mixed oxide catalyst for ammoxidation of propane to acrylonitrile, Fuel Process. Technol. 130 (2015) 71.